Human Molecular Genetics, 2017, Vol. 26, No. 10 1952–1965

doi: 10.1093/hmg/ddx066
Advance Access Publication Date: 3 March 2017
Original Article

ORIGINAL ARTICLE

AAV-mediated transfer of FKRP shows therapeutic efficacy in a murine model but requires control of gene expression

Evelyne Gicquel[1], Natacha Maizonnier[1], Steven J. Foltz[2], William J. Martin[3], Nathalie Bourg[1], Fedor Svinartchouk[1,†], Karine Charton[1,‡], Aaron M. Beedle[2,4] and Isabelle Richard[1,*]

[1]INSERM, U951, INTEGRARE Research Unit, Généthon, Evry, F-91002, France, [2]Pharmaceutical & Biomedical Sciences, University of Georgia College of Pharmacy, Athens, GA 30602, USA, [3]Animal Health Research Center, University of Georgia, Athens, GA 30602, USA and [4]Pharmaceutical Sciences, Binghamton University SUNY, Binghamton, NY 13902, USA

*To whom correspondence should be addressed at: Généthon, 1 rue de l'Internationale, 91000 Evry, France. Tel: 33-1 69472938; Fax: 33-1 60778698; Email: richard@genethon.fr

Abstract

Limb Girdle Muscular Dystrophies type 2I (LGMD2I), a recessive autosomal muscular dystrophy, is caused by mutations in the Fukutin Related Protein (FKRP) gene. It has been proposed that FKRP, a ribitol-5-phosphate transferase, is a participant in α-dystroglycan (αDG) glycosylation, which is important to ensure the cell/matrix anchor of muscle fibers. A LGMD2I knock-in mouse model was generated to express the most frequent mutation (L276I) encountered in patients. The expression of FKRP was not altered neither at transcriptional nor at translational levels, but its function was impacted since abnormal glycosylation of αDG was observed. Skeletal muscles were functionally impaired from 2 months of age and a moderate dystrophic pattern was evident starting from 6 months of age. Gene transfer with a rAAV2/9 vector expressing *Fkrp* restored biochemical defects, corrected the histological abnormalities and improved the resistance to eccentric stress in the mouse model. However, injection of high doses of the vector induced a decrease of αDG glycosylation and laminin binding, even in WT animals. Finally, intravenous injection of the rAAV-*Fkrp* vector into a dystroglycanopathy mouse model due to Fukutin (*Fktn*) knock-out indicated a dose-dependent toxicity. These data suggest requirement for a control of FKRP expression in muscles.

Introduction

The 'Dystroglycanopathies' regroup different genetic pathologies leading to secondary aberrant glycosylation of α-dystroglycan (αDG). This protein, mostly present in skeletal muscle, heart, eye and brain tissues, is a hyper-glycosylated membrane protein, the glycosylation process raising its weight from 70 to 156 kDa in muscle (1). It is part of the dystrophin-glycoprotein complex which connects the cytoskeleton to the extracellular matrix (ECM). Its high glycosylation level enables αDG direct binding to the laminin globular domains of some ECM proteins (2–4), such as laminin in the cardiac and skeletal muscles (5), agrin and perlecan at the neuromuscular junction (6,7), neurexin in brain (8)

[†]Present address: UMR U1179, F-78180 Montigny-le-Bretonneux.
[‡]Present address: AFM, Direction Scientifique, Evry, F-91002, France.
Received: December 7, 2016. **Revised:** February 16, 2017. **Accepted:** February 17, 2017

and pikachurin in the retina (9). Glycosylation of αDG is a complex process that is not yet fully understood [for a recent review see (10)]. Indeed, a number of genes have been identified as being involved in αDG glycosylation. These discoveries have been accelerating recently thanks to the use of high throughput sequencing methods for mutation detection in patients showing αDG glycosylation defects. One of these proteins is the Fukutin-Related Protein (FKRP). It was originally classified as a putative αDG glycosyltransferase on account of the presence in its sequence of a DxD motif, which is common to many glycosyltransferases, and evidence of αDG hypoglycosylation in patients mutated in the *FKRP* gene (11,12). Recently, FKRP and its homolog fukutin were identified as ribitol-5-phosphate (Rbo5P) transferases, forming a Rbo5P repeat linker necessary for addition of the ligand binding moiety (13).

Mutations in the *FKRP* gene can generate the entire range of pathologies induced by a defect in αDG glycosylation, from Limb-Girdle Muscular Dystrophy type 2I (LGMD2I; (14), Congenital Muscular Dystrophy type 1C (MDC1C; (12), to Walker-Warburg Syndrome (WWS) and Muscle-Eye-Brain disease (MEB); (15). There is an inverse correlation between the severity of the disease and the number of patients, the more severe, the rarer the patients (prevalence indicated in www.orphanet.fr: WWS (all genes): 1-9/1,000,000 and LGMD2I: 1-9/100,000). The type of pathology seems to be directly correlated to the nature of the *FKRP* mutation. In particular, the homozygous L276I mutation, replacing a leucine by an isoleucine in position 276 of the protein, is always associated with LGMD2I (16). LGMD2I is a recessive autosomal muscular dystrophy, affecting preferentially, albeit heterogeneously, the muscles of the shoulder and pelvic girdles. It is one of the most frequent LGMD2 in Europe, notably due to high prevalence of the L276I mutation in Northern Europe (17–19). The severity of the pathology is very heterogeneous. The muscular symptoms can appear between the first to third decades, and vary from Duchenne-like disease to relatively benign courses (14). The heart can also be affected with consequences such as severe heart failure and death (14,20–22). Investigations using cardiac magnetic resonance imaging suggest that a very high proportion of LGMD2I patients (60–80%) can present myocardial dysfunction such as reduced ejection fraction (23,24). Interestingly, the severity of the cardiac abnormalities is not correlated to the skeletal muscle involvement (20,24).

The present publication reports the generation and characterization of a new FKRP mouse model knock-in for the LGMD2I L276I missense mutation. The $FKRP^{L276I}$ mice proved to suffer from a mild and selective progressive dystrophy starting from the age of 6 months. This model was used to evaluate recombinant adeno-associated virus (rAAV) transfer of the *Fkrp* gene as a therapeutic approach. The rAAV serotype 9 was chosen since it is well known to target the skeletal muscle as well as the heart. This serotype was also used in the two previous studies where AAV-mediated FKRP transfer was reported (25,26). These studies used mostly an ubiquitous promoter to transfer FKRP either in neonates or 9 month-old animals with an additional study in neonates using muscle synthetic promoter for cardiac evaluation. In all these experiments, improvement of the muscle pathology was observed. Compared to these previous reports, our study is the first to analyze the consequences of a vector expressing FKRP under the control of a muscle-specific promoter (heart and skeletal muscles) in young adult mice, a situation that would resemble the situation that will be encountered in a clinical trial. We obtained strong expression of FKRP, at mRNA as well as protein levels, and showed the rescue of αDG proper glycosylation and increase in laminin binding, that led to histological and functional rescue of the dystrophy. However, injection of high doses of the vector [from 6.7 E10 to 1.2 E11 viral genome (vg)/TA] induced a decrease of αDG glycosylation and laminin binding even in WT animals. In these conditions, we observed an occasional immune response against the transgene as well as a dose dependent Endoplasmic Reticulum (ER)-stress. Furthermore, in another dystroglycanopathy model with skeletal muscle-specific knockout of the FKRP-homolog fukutin (FKTN), FKRP overexpression by rAAV9 injection appears to worsen the muscle pathology as indicated by increased central nucleation and, at high viral doses, substantially elevated endomysial fibrosis and increased macrophage infiltration. Altogether, these data support the possibility of using the AAV-mediated transfer of *FKRP* for treating LGMD2I and other FKRP deficiencies but indicate that high doses of expression should be avoided.

Results

Introducing the L276I mutation in the murine genome does not modify the expression of FKRP but leads to impairment of FKRP function

We created an animal model of LGMD2I ($FKRP^{L276I}$), introducing in the mouse genome the L276I mutation by homologous recombination using a plasmid containing the mutated *Fkrp* exon 3 flanked with a Neo cassette (Fig. 1A). Chimeric animals were obtained and the Neo cassette was excised by crossing with mice expressing the CRE recombinase under the control of a ubiquitous promoter. The mice were then interbred to generate homozygous mutated mice that were obtained at the expected Mendelian ratio. Quantitative RT-PCR (RT-qPCR) analyses performed on skeletal muscle revealed the same amount of *Fkrp* mRNA between wild type (WT) and $FKRP^{L276I}$ mice (Fig. 1B), indicating that the introduced mutation does not destabilize *Fkrp* mRNA.

To check the consequences at protein level, we developed a novel polyclonal FKRP antibody directed against an epitope located at the C-terminus of the human FKRP protein, and identical to the mouse sequence but for one amino-acid (Supplementary Material, Fig. S1A). A Western-blot performed on lysates of HER911 cells transfected with a *Fkrp* plasmid revealed 2 bands with different intensity and size (Supplementary Material, Fig. S1B, left panel). The minor band around 50–55 kDa corresponds to the predicted size of the FKRP polypeptide (54.8 kDa) and the major band at 58 kDa most likely to a N-glycosylated form of the protein, since it was previously reported that FKRP undergoes such post-translational modification (27). A similar pattern was also observed in human and mouse skeletal muscles (Supplementary Material, Fig. S1B, middle and right panels). In these samples, we also observed an additional band at 42 kDa. To clarify the nature of this band, we isolated the 58 and the 42 kDa bands from gel and treated them with cyanogen bromide, a product known to hydrolyze peptide bonds at the level of methionine residues. While the profile obtained after Western blot with the digested 58 kDa band fits with the position of methionine in the sequence of the FKRP protein, the digested 42 kDa band resulted in a totally different profile, excluding the possibility of corresponding to an isoform of FKRP (Supplementary Material, Fig. S1C) when considering the position of methionine in the sequence (Supplementary Material, Fig. S1A). Western-blot using this newly developed FKRP antibody showed no difference between WT and $FKRP^{L276I}$ mouse muscles, indicating that the introduction of the L276I mutation in mice did not alter the expression of *Fkrp* (Fig. 1C).

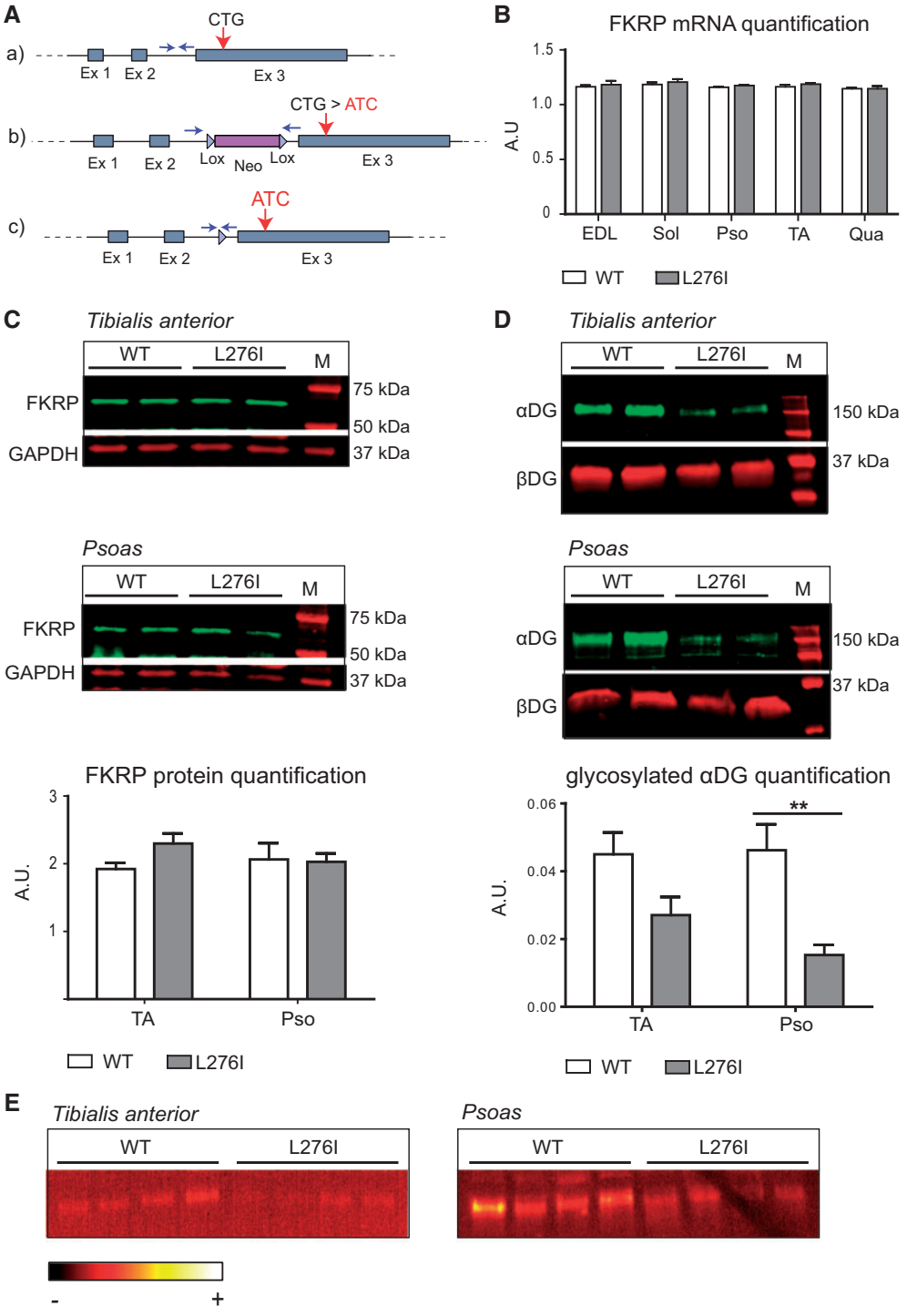

Figure 1. Generation and molecular characterization of FKRP^{L276I} mouse. **A**/(A) Representation of the *Fkrp* locus on mouse chromosome 7 with the position of the L276 codon (CTG) indicated. **(B)** Plasmid construct used for the homologous recombination. The floxed neomycine resistance cassette was inserted upstream of the third exon. The knock-in mutation (CTG > ATC) was introduced within the third exon. **(C)** Final recombinant *Fkrp* allele after deletion of the selection cassette by the CRE recombinase. Arrows represent the primers used for genotyping. (B)/Quantification of *Fkrp* mRNA by real-time PCR in WT and FKRP^{L276I} muscles normalized by the ubiquitous acidic ribosomal phosphoprotein (P0) mRNA ($n = 3$; values ± SEM). EDL, soleus (Sol), psoas (Pso), TA and quadriceps (Qua) muscles of 6 months old mice were assayed. AU= arbitrary unit. (C)/Expression of FKRP at protein level by Western-blot on TA and psoas muscles of 2 months old WT and FKRP^{L276I} mice. GAPDH (Glyceraldehyde-3-Phosphate Dehydrogenase) was used as loading control. M= molecular marker. Quantification is shown below the western blots. **(D)**/Western-blot of glycosylated αDG using IIH6 antibody on TA and psoas muscles of 2 months old WT and FKRP^{L276I} mice. β-dystroglycan (βDG) was used as loading control. M= molecular marker. Quantification is shown below the western blots. **(E)**/Laminin overlay on TA and psoas muscles of 2 months old WT and FKRP^{L276I} mice. The ImageJ 'RedHot' false color scheme was applied to the image.

The function of mutated FKRP was then explored. Western-blots of αDG were performed on WT and FKRP^{L276I} muscles, revealing a decreased amount of the fully glycosylated αDG band between WT and FKRP^{L276I} muscles (Fig. 1D). Laminin overlay was performed on normal and mutated gluteus muscles and revealed a decrease in the binding between laminin and αDG for FKRP^{L276I} muscles (Fig. 1E). These results indicated that the introduction of the mutation has impaired the function of FKRP.

The L276I mutation impairs the resistance of the muscle to eccentric stress

Histological analysis of all observed muscles [tibialis anterior (TA), gastrocnemius, soleus, quadriceps, psoas, deltoid, diaphragm, gluteus, extensorum digitorum longus (EDL), biceps brachii] showed no sign of dystrophy until the age of 6 months. At this age, small clusters of centronucleated fibers, an indication that they had undergone regeneration, started to be observed that further increased with age (Fig. 2A). The number of centronucleated fibers of 6 month-old FKRP^{L276I} mouse muscles was quantified and was found to be significantly elevated compared to WT mice in the proximal muscles, psoas and gluteus, but not in the distal muscles, TA and gastrocnemius (Fig. 2B). We also measured the fiber diameter and observed an increase in fiber size in some muscles such as the gluteus (Fig. 2C). Hypertrophy was also observed in the EDL (15.66 mg ± 1.24 for FKRP^{L276I} versus 12.81 mg ± 1.37 for WT) and soleus muscles (13.11 mg ± 1.56 for FKRP^{L276I} versus 11.17 mg ± 1.63 for WT) while specific force of these muscles did not show any difference as evaluated by *ex vivo* measurement (EDL: 17.62 mN/mg ± 4.19 for FKRP^{L276I} versus 20.20 mN/mg ± 2.94 for WT; soleus: 18.54 mN/mg ± 3.62 for FKRP^{L276I} versus 17.26 mN/mg ± 2.75 for WT). This characterization indicates that the FKRP^{L276I} mice showed moderate muscular dystrophy with selectivity of impairment. Additionally, we investigated the heart. No histological defects were detected before 9 months, the age at which some mice started to show abnormalities. When quantified at an age between 12 and 15 months, 5 out of 14 mice presented multifocal areas of interstitial fibrosis (Fig. 2D, middle panel) while the others showed no histological abnormalities (Fig. 2D, right panel). Heart weights of 12 month-old mice vary significantly (P-value = 0.01) from 198 mg in control littermate mice ($n = 9$, SD = 32) to 237 mg in FKRP^{L276I} mice ($n = 8$ SD = 30), indicating an adaptive response to FKRP deficiency.

We explored the muscle resistance in FKRP^{L276I} mice using an eccentric protocol (large strain injury or LSI) (28,29) using mice at 2 months of age. The stress was applied on the left ankle dorsiflectors, consisting of TA and EDL muscles. Mice were injected with Evans blue dye and sacrificed 24 h after LSI (Fig. 2E). Quantification of Evans blue dye labelling revealed a larger area of impairment in FKRP^{L276I} mouse muscles than in WT mouse muscles, underlining a greater vulnerability to eccentric stress for muscles of FKRP^{L276I} mice. These results indicate that the fragility of FKRP^{L276I} muscle fibers is already present at 2 months of age and therefore occurs much earlier than the appearance of the first histological signs of dystrophy.

AAV-mediated FKRP gene transfer rescues the molecular and functional impact of the L276I mutation

To restore the function of FKRP in the muscles of FKRP^{L276I} mice, we constructed and administered a rAAV2/9 vector expressing the murine FKRP (AAV9-*mFkrp*) to FKRP^{L276I} mice (Fig. 3A). First, the vector was injected intramuscularly in gastrocnemius and gluteus muscles of 2 month-old FKRP^{L276I} mice, with a dose of 2.6 E10 vg per muscle. After 1 month, muscles were sampled and the impact of the transfer on FKRP expression, αDG glycosylation and laminin binding were assessed. Overexpression of FKRP after gene transfer was confirmed by Western blot, as weak in gastrocnemius and more important in gluteus (Fig. 3B). Western blot performed with IIH6 antibody showed a more intense labelling of αDG in injected FKRP^{L276I} muscles compared to non-injected FKRP^{L276I} muscles, indicating that αDG glycosylation was restored (Fig. 3B). Laminin overlay on gastrocnemius and gluteus muscles also pointed to a restoration of laminin binding in AAV-injected conditions (Fig. 3C). We also applied LSI eccentric exercise to 2–3 month-old FKRP^{L276I} mice that had previously been injected intramuscularly into the TA muscle with AAV9-*mFkrp* with a dose of 1.5 E10 vg. Interestingly, we found that the injured area decreased in muscles treated with the vector, compared to non-injected muscles (Fig. 3D). Thus, AAV9-*mFkrp* effectively protected FKRP^{L276I} muscles from eccentric stress.

AAV9-*mFkrp* was then administered by systemic injection into the tail vein of 1 month-old FKRP^{L276I} mice with a dose of 5 E12 vg/kg. Muscles and hearts were sampled 5 months post-injection. We first assayed the transduction efficacy in various muscles including the psoas and gluteus muscles, the most affected muscles, using AAV vector copy number quantification, and noted that gene transfer had been efficient in psoas but not in gluteus muscles (Fig. 4A and Supplementary Material, Fig. S2). Note that the gluteus is a muscle with a low level of vascularization in mice and, accordingly, a low transfer is often seen in our tail vein injection experiments. Western blots for FKRP and αDG were performed on the psoas of systematically injected mice. The expression of FKRP was slightly increased and the glycosylation of αDG was found restored almost at the level of WT muscles (Fig. 4B). Histological benefits were assessed in affected muscles (psoas and gluteus) at 6 months of age, therefore 5 months after systemic injection. A decrease in the number of centronucleated fibers was observed only in psoas muscle but not in gluteus muscle (Fig. 4C). This observation indicates that, in muscles efficiently transduced by AAV9-*mFkrp*, the vector succeeded in reducing the FKRP^{L276I} dystrophic impairment.

In the heart, the 58 kDa FKRP band appears with high intensity, whereas it is undetectable in the non-injected condition (Fig. 4D). We then analyzed the cardiac histology to ensure that this high expression in the heart would not lead to deleterious effects. No abnormality was observed, consistent with the absence of cardiac phenotype of the FKRP^{L276I} mice at that age and with an absence of deleterious effect of the expression of FKRP (Fig. 4E).

FKRP overexpression modifies the link between ECM and the sarcolemma in a dose-dependent mode

To explore the effect of FKRP overexpression on its localization and function, we injected AAV9-*mFkrp* into TA muscles of WT mice with two different doses: 1.5 E10 vg/TA, and 1.2 E11 vg/TA. We confirmed a dose-dependent expression of FKRP at mRNA and protein levels (Fig. 5A). We assessed FKRP function on αDG glycosylation in FKRP-overexpressing muscles by evaluating αDG glycosylation by Western-blot using the IIH6 antibody (Fig. 5A). We detected αDG at the expected size, but surprisingly, the injected muscles presented a variation in IIH6-αDG labelling depending on the dose. We first observed an increase in the intensity of glycosylation with the lowest dose and a decrease

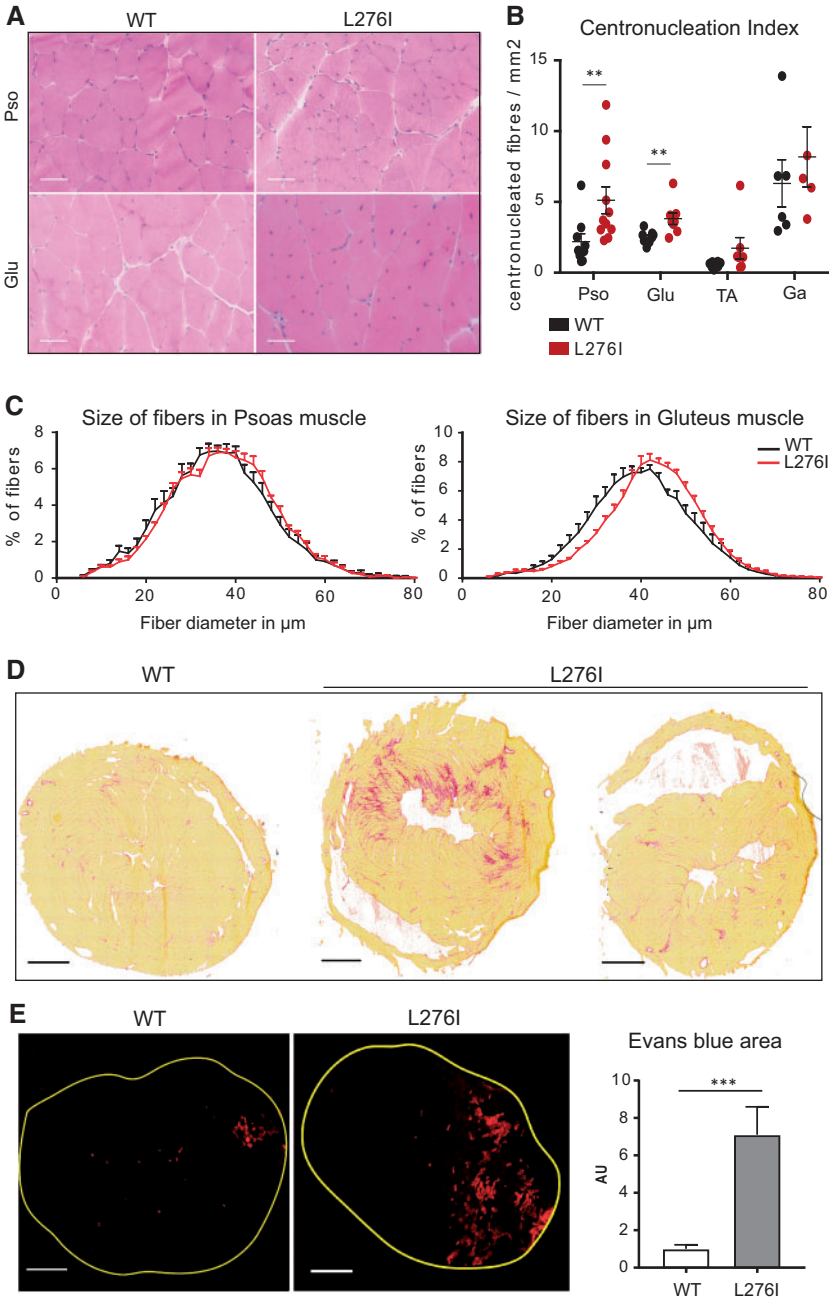

Figure 2. Histological and functional characterization of FKRP^{L276I} mouse. **(A)**/HPS histological staining of psoas (Pso) and gluteus (Glu) muscles, from WT and FKRP^{L276I} mice at 6 months of age. Scale bars = 50 µm. **(B)**/Number of centronucleated fibers per mm2 in gluteus (Glu), psoas (Pso), TA and gastrocnemius (Ga) muscles of WT and FKRP^{L276I} mice at 6 months of age ($n = 5$ to 11). ROUT and Grubbs outlier tests were performed with only the ROUT test indicating one outlier in the psoas data. Note that Mann-Whitney statistical test without this point gives similar significance (**; P-value = 0.008931). **(C)**/Distribution of fiber diameter size in psoas and gluteus muscles of WT and FKRP^{L276I} mice at 6 months of age ($n = 8$). A shift towards larger fibers is observed in FKRP^{L276I} muscles. **(D)**/Sirius red staining of hearts of 12-month-old WT and FKRP^{L276I} mice. Scale bars = 1 mm. **(E)**/Evans blue dye fluorescence in the left ankle dorsiflectors of WT ($n = 12$) and FKRP^{L276I} ($n = 13$) mice at 2 months of age, after LSI. Scale bars = 500 µm. The graph on the right represents the quantification of the area labeled with Evans blue dye in left ankle dorsiflector sections after LSI, normalized to the data of WT mice. Error bars represent SEM.

with the highest dose compared to PBS-injected animals. These data indicate a glycosylation defect of αDG in the high FKRP overexpression condition. We then performed a laminin overlay on the same samples to evaluate the binding between αDG and laminin. This experiment showed an increase in the fixation of laminin on αDG at the lowest dose (Fig. 5A) and a decrease of the binding for the highest dose (Fig. 5A). A similar experiment was performed on FKRP^{L276I} with similar outcomes (Supplementary Material, Fig. S3). Quantification of α-DG glycosylation and of laminin binding capacity for these 2 experiments are presented in Supplementary Material, Figure S4. Note that that, even if the quantification level is not significantly different between the control and the highest dose, the gel profile of glycosylation and/or laminin binding appear different (Fig. 5). To confirm that the observed effect was related to FKRP overexpression but not to the high dose of AAV vector, we performed a

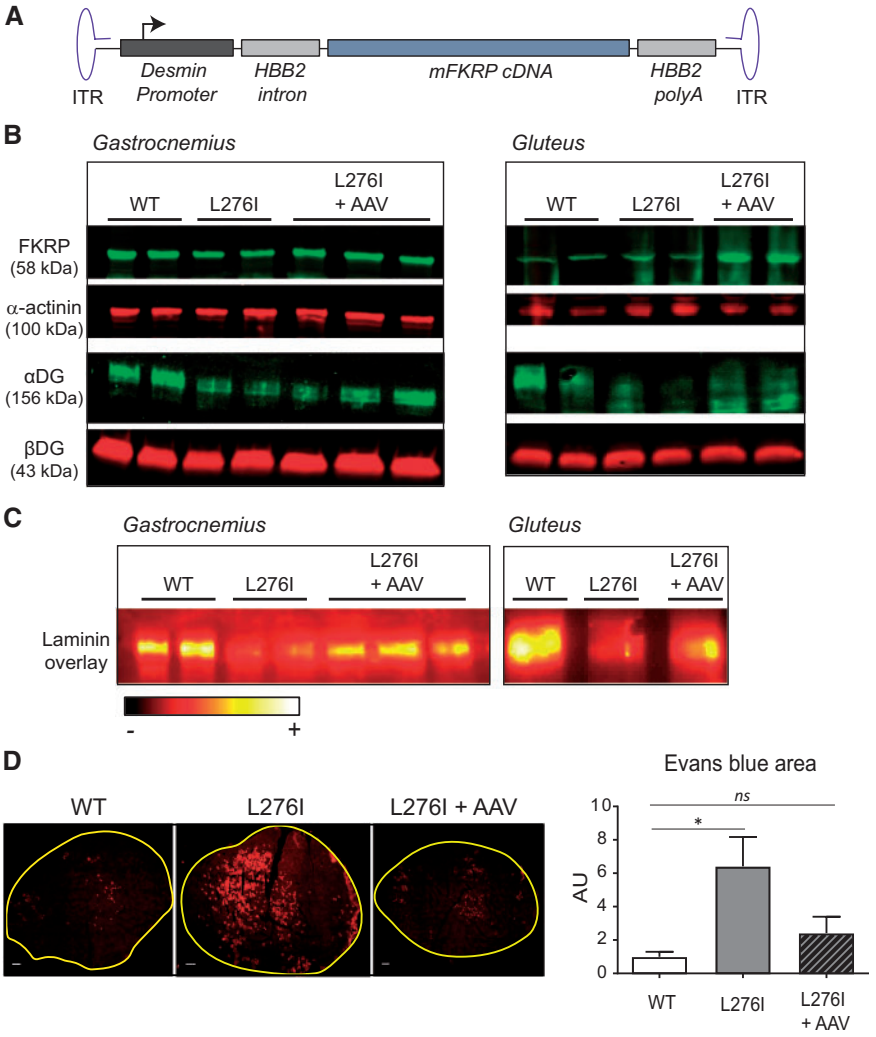

Figure 3. Intramuscular *Fkrp* gene transfer in FKRP^{L276I} mouse. **(A)**/Schematic representation of AAV9-*mFkrp* genome. The *mFkrp* cDNA is under the control of the desmin promoter. HBB2 = (Hemoglobin subunit β2). **(B)**/Expression of FKRP and level of glycosylated αDG by Western-blot on non-injected and AAV-injected mice 1 month after injection. Both gastrocnemius (Ga) and gluteus (Glu) muscles were assayed. Loading controls are α-actinin for FKRP and βDG for αDG. **(C)**/Laminin overlay on injected and non-injected muscles. Both gastrocnemius (Ga) and gluteus (Glu) muscles were assayed. The ImageJ 'RedHot' false color scheme was applied to the images. **(D)**/Evans blue dye fluorescence in the left ankle dorsiflectors of WT, PBS-injected FKRP^{L276I} and AAV-injected FKRP^{L276I} mice at 2–3 months of age, after LSI. Scale bars = 500 μm. The graph on the right represents the quantification of the area labeled with Evans blue dye in left ankle dorsiflector sections after LSI, normalized to the data in WT mice ($n = 9$; values ± SEM); ns= not significant.

control experiment where WT mice were injected in the TA with different doses of AAV not coding for any protein. No change in glycosylation or decrease in laminin-binding was observed, confirming that the effect observed at the high dose with the FKRP vector was due to FKRP expression (Supplementary Material, Fig. S5).

We then analyzed the consequences of FKRP overexpression at the histological level and observed no disruption of the histology apart from noticeable inflammatory infiltrates on TA section of one WT animal injected with the highest dose (Fig. 5B and Supplementary Material, Fig. S3). We qualified this response as cytotoxic T-lymphocytes and macrophages by immunostaining, suggesting an immune response to the transgenic protein (Fig. 5C). Since it was previously shown that a link between FKRP and ER stress exists (30,31), we analyzed the level of 78 kDa glucose regulated protein (GRP78), a protein central to the ER-response, by western blot. We observed an upregulation of this marker in the condition where the glycosylation and laminin binding were abnormal (Fig. 5D).

FKRP overexpression can be deleterious when injected in a fukutin animal model

Since we observed an increase in glycosylation of αDG with the low dose of FKRP, we investigated the possibility of compensation for defects associated with abnormal glycosylation of αDG with decreased extracellular ligand binding activity, such as the fukutin (FKTN) deficiency. Previous work indicated that up-regulation of LARGE, another protein involved in αDG glycosylation was beneficial in dystroglycanopathies (1). The skeletal muscle specific Myf5/Fktn Cre/LoxP knockout mouse model is a moderate to severe model of dystroglycanopathy with early lethality at approximately 18–24 weeks of age (32). Four week-old male and female

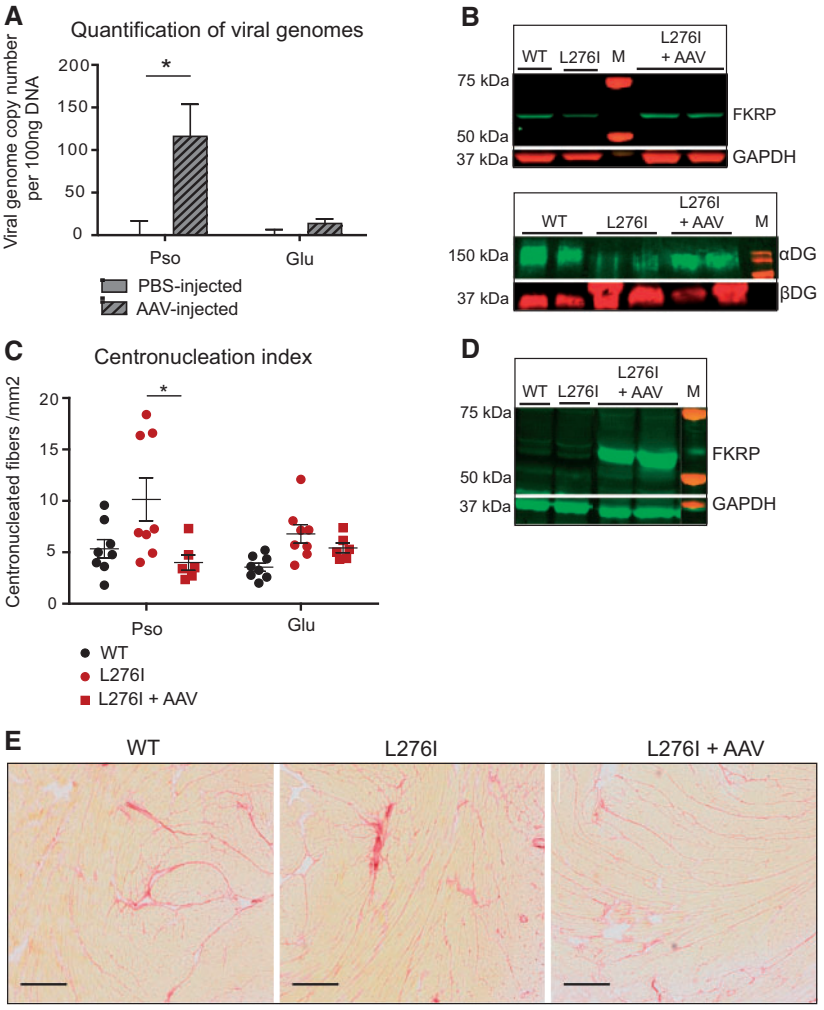

Figure 4. FKRP gene transfer in FKRP^{L276I} mouse by intravenous administration. **(A)**/Quantification of viral genome number using qPCR, in psoas (Pso) and gluteus (Glu) muscles of intravenously injected mice, either with PBS ($n = 4$) or with AAV9-*mFkrp* ($n = 6$). **(B)**/Upper panel: expression of FKRP by western-blot on the psoas muscle of intravenously injected mice, either with PBS or with AAV9-*mFkrp*. GAPDH is used as loading control. Lower panel: level of glycosylated αDG by western-blot on non-injected and AAV-injected mice in psoas muscle. βDG is used as loading control for αDG. M = molecular marker. **(C)**/Number of centronucleated fibers per mm2 in psoas (Pso) and gluteus (Glu) of non-injected ($n = 8$) or intravenously injected with AAV9-m*Fkrp* mice ($n = 6$). ROUT and Grubbs outlier tests were performed without indicating any outlier. **(D)**/Expression of FKRP by western-blot on hearts of non-injected and intravenously AAV9-m*Fkrp* injected mice. M = molecular marker. **(E)**/Sirius red coloration of hearts of non-injected and intravenously AAV9-m*Fkrp* injected mice, showing that even if a high expression level of FKRP is seen in heart after IV injection, it has no consequences on the histological aspect of the tissue. Scale bars = 50 μm.

Myf5/Fktn deficient and littermate mice were injected intravenously with low or high doses of rAAV9-*mFkrp* (5 E12 vg/kg and 10 E12 vg/kg). The low dose corresponds to the dose with which we observed a beneficial effect in the FKRP^{L276I} mice. Interestingly, the outcome of the AAV injection was different between the littermate control mice, which demonstrated weaker expression of FKRP, and the *Fktn* knock-out mice, which had a markedly higher expression of FKRP at both doses. Consistent with the FKTN deficit, the glycosylation of αDG was typically reduced in the *Fktn* knock-out and was not restored after AAV9-*mFkrp* injection (Fig. 6A). No change regarding the glycosylation was observed in the WT mice with or without injection (Fig. 6A).

At the histological level, no abnormality was observed in the WT psoas, but a dose-dependent worsening of the dystrophic features was evident in the Myf5/Fktn knock-out mice as demonstrated by an increase in centrally nucleated fibers, a proliferation of endomysial connective tissue and a breakdown of the muscle tissue (Fig. 6B). In addition, we checked for involvement of macrophage and lymphocyte immune cell infiltration in the Myf5/Fktn mice 4 weeks post-AAV injection. We could not detect lymphocyte marker CD3 in the psoas of any study mice (data not shown). Notably, macrophage marker CD11b was increased in high dose AAV-treated Myf5/Fktn knock-out mice (Fig. 6C). It seems therefore that FKRP injection can lead to a worsening of the dystrophic process in an already damaged muscle.

Discussion

In this study, we showed that the introduction of the L276I mutation in the FKRP protein has no impact on its expression at transcriptional or at protein levels in mice and does not modify the *N*-glycosylation of FKRP. Interestingly, it was previously shown that a L276I mutated protein expressed *in vitro* could be detected predominantly in the Golgi apparatus whereas other

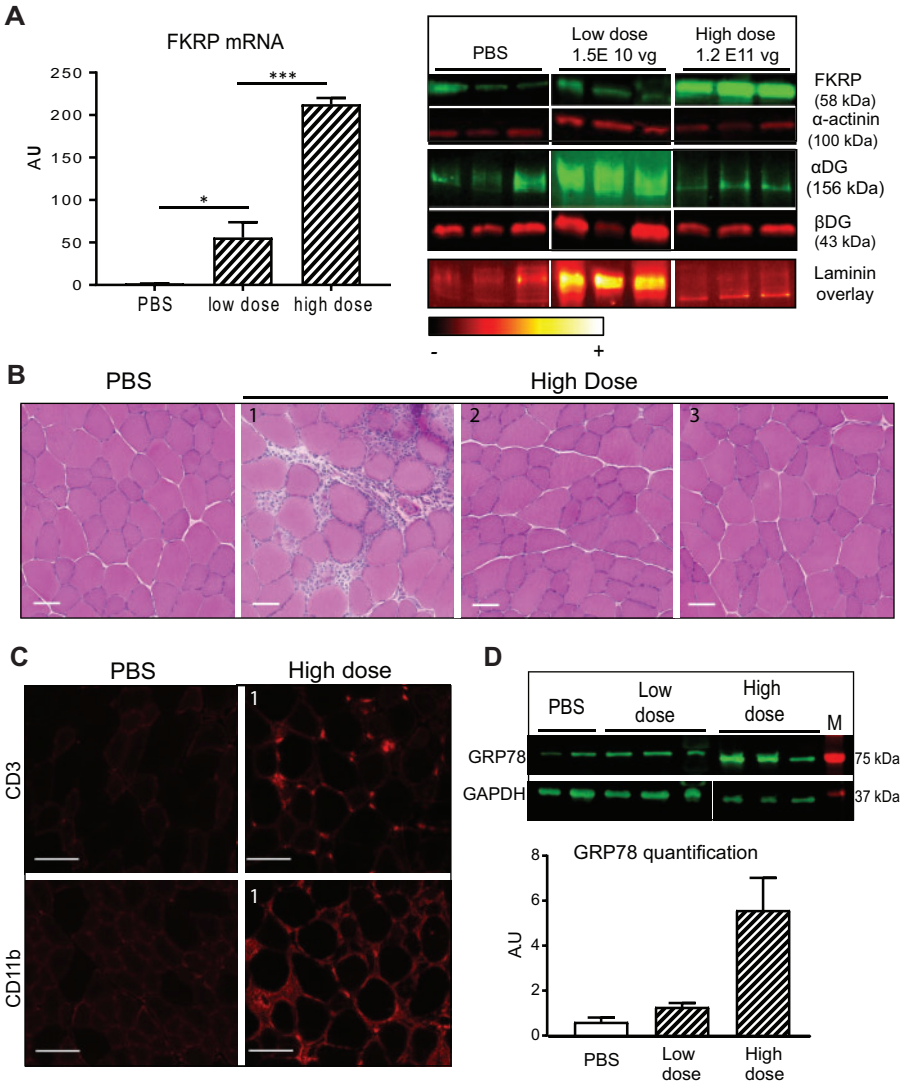

Figure 5. Consequences of injection of different doses of *Fkrp* in WT mice. **(A)**/Molecular analyses of TA muscle after transfer of different doses of AAV9-m*Fkrp* (low dose =1.5 E10 vg/TA and high dose =1.2 E11 vg/TA). Left panel: Quantification of FKRP mRNA using RT-qPCR in TA muscles injected with the 2 doses. Right panel from top to bottom: FKRP expression and control of protein loading using α-actinin, αDG labelling using IIH6 antibody and βDG as control, and laminin binding overlay in ImageJ 'RedHot' false color scheme. **(B)**/Histological section of TA after gene transfer. One animal out of three WT injected with the high dose showed inflammatory infiltrates. Scale bars = 50 μm. **(C)**/Immunostaining with CD3 and CD11b antibodies, indicating the presence of lymphocytes and macrophages respectively in the inflammatory infiltrate. Scale bars = 50 μm. **(D)**/Expression of GRP78 at protein level in animals injected with the different doses of AAV9-m*FKRP*, and GAPDH as control of protein loading. M = molecular marker. Quantification of GRP78 normalized with GAPDH ($n = 3$). A.U. = arbitrary unit.

mutations (P448L, S221R, A455D) causing the more severe congenital muscular dystrophy phenotypes were retained in the ER (33,34). Additional experiments showed that the immunolabelling pattern of FKRP in the muscle of LGMD2I patients homozygous for this mutation is indistinguishable from normal biopsies (35). Here, we demonstrated that the mutation has a clear impact on the function of the protein and therefore that this residue is important either for its functional activity or for substrate recognition in the Golgi apparatus.

The FKRP^{L276I} model turned out to suffer from a moderate form of muscular dystrophy, similar to the phenotypes of previously described mouse models carrying this particular mutation (26,36). Interestingly, we identified a test that highlighted the exacerbated fragility of FKRP^{L276I} muscles to eccentric stress and showed that the functional defect is already present in the mouse at 2 months of age, long before the onset of the muscular dystrophy features on biopsies. This observation indicates an intrinsic frailty of the muscle, possibly caused by lack of resistance of the cell membrane containing a partially glycosylated αDG that binds less to laminin in the ECM.

Injections of AAV9-*mFkrp* resulted in up-regulation of transgenic *Fkrp* mRNA, leading to overexpression of the N-glycosylated form of FKRP. Histological improvement of muscles that efficiently received viral vector after systemic administration at a dose of 5 E12 vg/kg was observed, as well as better resistance to eccentric stress. These results indicate an improved phenotype after *Fkrp* gene transfer. Furthermore, since the vector was injected at a time when the susceptibility to damage induced by mechanical stress is present but the pathology is not yet evident at histological level, our data suggest that both the susceptibility and the subsequent degenerative dystrophic process can be prevented. AAV-mediated transfer of FKRP was previously reported in different settings and models (25,26). In a first study, an AAV9 expressing FKRP under a ubiquitous promoter was injected in

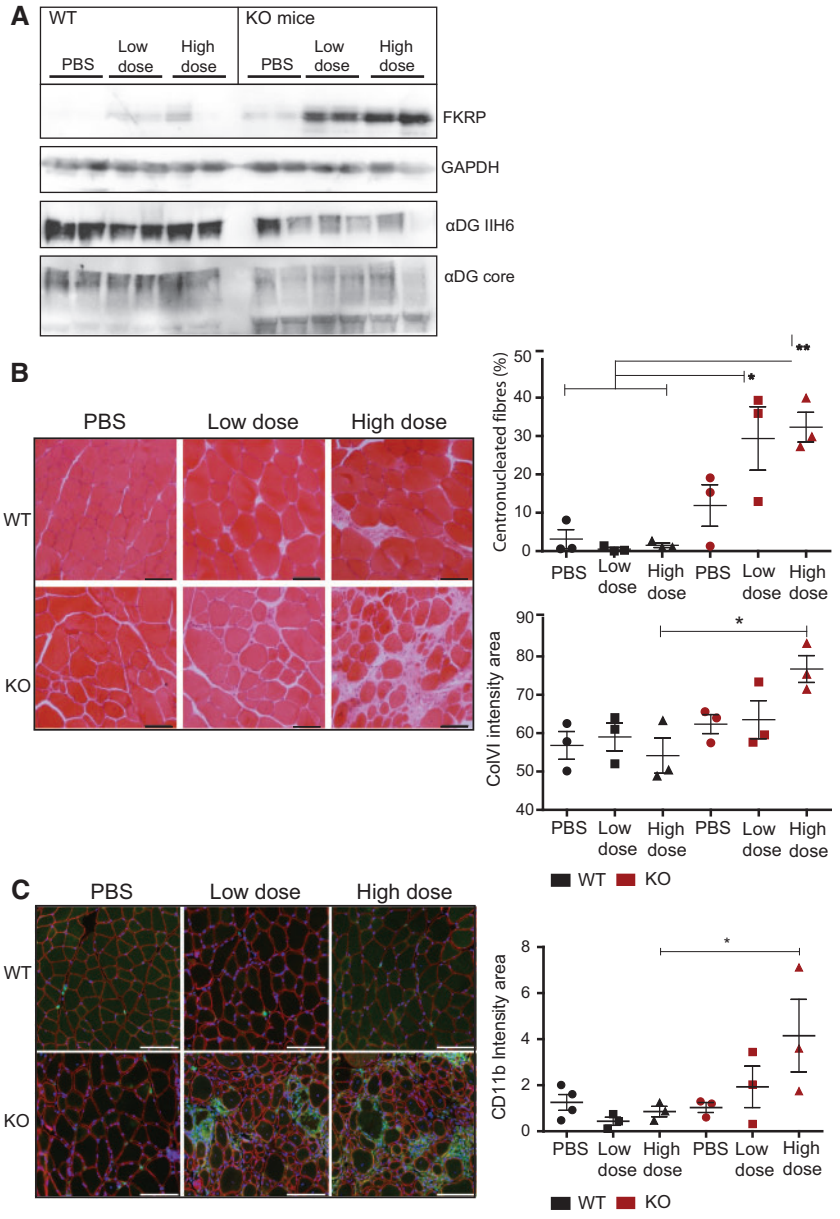

Figure 6. FKRP gene transfer in skeletal muscle-specific Myf5-cre *Fktn* knockout mice. **(A)**/Molecular analyses of pooled hindlimb muscle from 8 week-old mice, 4 weeks after intravenous transfer of different doses of AAV9-m*Fkrp* (2 E12 vg/kg and 4 E12 vg/kg). From top to bottom: αDG glycosylation (IIH6 antibody), αDG core protein, FKRP expression (Rbt341) and GAPDH as control. **(B)**/Left panel: Hematoxine-Eosine staining on histological section of psoas muscle after gene transfer. Scale bars = 100 μm. Right upper graph: percentage of centronucleated fibers in injected mice muscles. Right lower graph: quantification of fibrosis as ColVI intensity (green) of the entire psoas normalized by psoas area ($n = 3$). **(C)**/CD11b macrophage marker increased in Myf5-cre *Fktn* knockout mice 4 weeks after high dose *Fkrp* gene transfer. Left panel: immunostaining of psoas with CD11b (green), βDG (red) and DAPI nuclear counterstain (blue). Scale bars = 100 μm. Right graph: quantification of CD11b (green, mean fluorescent intensity) of entire psoas normalized by psoas area. ($n = 3$–4) * $P < 0.05$. Error bars represent SEM.

3–4 weeks-old mice knock-in for the P448L mutation by intraperitoneal (IP) injection at a dose of 5 E11 vg/mouse (25) and the effects analyzed 4 months after injection. A second study also used AAV9 expressing FKRP under the control of a ubiquitous promoter but this time in L276I knock-in mice. Neonates were injected at a dose of 1 E11 vg/mouse IP and 9 month old animals at a dose of 6 E13 vg/kg IV (26). In addition, an AAV expressing FKRP under the control of a synthetic promoter was used in neonate for evaluation of cardiac function. Our study was the first to evaluate the beneficial effect at the skeletal muscle level of a vector expressing FKRP under the control of a muscle-specific promoter in young adult mice. In addition, the dose that we used was one order of magnitude lower than in the systemic experiment presented in (26). These two elements are of importance when considering application of the AAV-mediated transfer in gene therapy clinical trial.

Interestingly, we observed an increase of the αDG laminin binding at moderate dose in wild-type and FKRP^{L276I} animals suggesting that FKRP can enhance the link between the sarcolemma and the ECM. This prompted us to test the possibility of compensation in the FKTN deficient mouse model, for the following reasons. First, FKTN and FKRP are homologs; therefore, they are most likely to have overlap in function. Second, overexpression of like-acetylglucosaminyltransferase (LARGE), a

crucial glycosyltransferase for extension of the final laminin binding disaccharide repeat on the αDG O-mannose glycan, has been proposed as a therapeutic strategy to enhance the laminin-binding activity of αDG and therefore to compensate αDG hypoglycosylation caused by the defects of other αDG glycosyl-transferases. Related studies provided support for the concept that overexpression of one αDG processing enzyme might compensate for loss of another (37–41). However, we observed that high doses of FKRP can have abnormal consequences. It modified or reduced the recognition of the glycosylated epitope by IIH6 antibody on αDG and precluded the binding of αDG with its laminin ligand. In addition, it worsened the condition in highly dystrophic model Myf5/*Fktn*, suggesting the FKRP expression could be deleterious in conditions where the muscles is already highly damaged. Further experiements would be required to consolidate this information in additional models. It is possible that FKRP overactivity may direct the glycosylation in an abnormal direction in a dominant negative fashion, leading to glycosylated moieties which are not recognized by the IIH6 antibody and have reduced laminin binding.

The molecular effect of the decrease in glycosylation of αDG and in laminin binding when FKRP is overexpressed was observed both in WT and $FKRP^{L276I}$ mice but with no deleterious consequences on muscles. In particular, treated muscles showed no evidence of decreased resistance to eccentric contractions. Moreover, we followed up treated mice until the age of 6 months and did not observe mortality or deleterious histological signs in the skeletal or cardiac muscles. Additional experiments with a longer time frame are now on-going. Interestingly, detailed muscle physiological analysis demonstrated a loss of force in response to eccentric exercise in LARGE-overexpressing mice at 8 months of age, but without association with any morphological changes (38). In addition, the identification of patients with *FKRP* and *FKTN* mutations and relatively mild muscle phenotypes despite absent IIH6 labelling suggests that disruption of the laminin-αDG interaction in muscle, as recognized by the IIH6 antibody, does not correlate obligatorily with pathological effects (42). Our data confirmed the absence of correlation between profound depletion of αDG and phenotype. In contrast, transfer of *Fkrp* in the context of highly dystrophic model such as the Myf5/Fktn mice leads to worsening of the phenotype. This is reminiscent of what was observed by overexpression of LARGE in dy2J (laminin a2 deficiency) and *Fktn* knock-out mice (43). The idea that dystrophic muscle undergoing regeneration may be more susceptible to modification of the equilibrium of glycosylation is consistent with the fact that αDG glycosylation is a crucial process during development and muscle regeneration (44). Examination of the overexpression of FKRP in a more advanced FKRP model is now on-going to determine whether any aggravation of the phenotype could occur.

In conclusion, our data further confirm previous studies on the consequence of the L276I mutation *in vivo* and on the positive effect of *FKRP* transfer. However, we also showed that control of expression of FKRP would be mandatory, possibly because of the extreme sensitivity of αDG glycosylation to an optimal range of enzyme level.

Materials and Methods

Generation and genotyping of $FKRP^{L276I}$ mice

Construction of the targeting vector and generation of the murine knock-in model for the L276I FKRP mutation were performed at the 'Mouse Clinic Institute' according to standardized protocols (MCI/ICS, Illkirch). Two PCRs were performed to amplify exon 3 on both sides of the mutation site, with primers containing the L276I FKRP mutation. The 2 generated fragments were assembled during a third PCR and cloned into the targeting vector, a MCI proprietary vector containing a loxed Neomycin resistance cassette. Two fragments of 3.5 kb (corresponding to the 5′ and 3′ homology arms) were amplified by PCR and subcloned directly upstream and downstream of the cassette in the previous plasmid to generate the final targeting construct. The plasmid sequence was verified by restriction digest and sequencing of every exon and exon-intron junction. The linearized construct was electroporated in 129Sv/Pas mouse embryonic stem (ES) cells, and G418-resistant colonies were isolated and expanded. After selection, 372 clones were screened by PCR using external primers and further confirmed by Southern blot with 5′ and 3′ external probes. Two clones were found to carry the desired modification. The correctly modified ES clones were injected into C57BL/6J blastocysts that were reimplanted into foster mothers to generate the chimeric F0 mice. The male chimeras were bred with transgenic females for CMV-CRE to excise the neo cassette. The Cre transgene was segregated out by a first cross on C57BL/6 background; the resulting heterozygous mice were backcrossed for 3 generations and then interbred. The presence of the introduced mutation (CTG > ATC) was confirmed by sequencing. For genotyping, genomic DNA from mouse tail was extracted and amplified using REDExtract-N-Amp Tissue PCR Kit (Sigma, St. Louis, MO, USA) with the following primers chosen in the *Fkrp* gene: 1345.s: 5′-GCCTGATGTCAGACCCTAGCTG-3′ and 1344.as: 5′-GGAAAAGTGACCCCATGACGTGATG-3′. The resulting WT and mutant alleles generated PCR fragments of 212 and 300 bp, respectively. In each experiment, normal littermates of $FKRP^{L276I}$ mice were used as control. All mice were handled according to the European guidelines for the human care and use of experimental animals, and all procedures on animals were approved by Genethon's ethics committee under the number CE11-012. Animals were housed in a barrier facility with 14-h light, 10-h dark cycles, and provided food and water *ad libitum*. In this study, only male mice were used.

Skeletal muscle-specific Fktn knockout mice

Floxed *Fktn* exon 2, containing the start codon, was deleted during skeletal muscle specification by Myf5-cre, as previously described (32,45). $Myf5^{cre/+}$,$Fktn^{L/+}$ mice were bred to $Fktn^{L/L}$ mice to generate knockout (Myf5/Fktn KO: $Myf5^{cre/+}$,$Fktn^{L/L}$) and littermate control mice (LC: $Fktn^{L/+}$, $Fktn^{L/L}$, or $Myf5^{cre/+}$, $Fktn^{L/+}$ littermates). Genotyping was carried out as described previously and both male and female mice were used without preference as the phenotypic range is similar between the sexes (32). Mice were maintained on a 12 h:12 h light:dark cycle. *Ad libitum* food pellets and water were supplemented with wet gruel (water soaked food pellets) on the floor of the cage 2–3 times per week. All mouse husbandry and experimental procedures were approved by the University of Georgia IACUC committee.

Plasmids and AAV vectors

The coding sequence of murine *Fkrp* was amplified from the IMAGE clone AK114, using an upstream primer containing an EcoRI restriction site (in bold): 5′-CG**GAATTC**CGATGCGG CTCACCCGCTGCTG-3′ and a downstream primer carrying XhoI restriction site (in bold): 5′-CCG**CTCGAG**CGGTCAACCGCCT GTCAAGCTTA-3′. This PCR product was cloned using the

ZeroBlunt TOPO XL PCR Cloning Kit (Thermo Fisher Scientific, Waltham, MA, USA) to obtain the plasmid pCR-BluntII-m*Fkrp*. After digestion with the restriction enzymes EcoRI and XhoI, the fragment was subcloned into an AAV-based pSMD2-derived vector carrying type 2 ITR to obtain the plasmid pAAV-Des-m*Fkrp*, where m*Fkrp* is placed under the control of the desmin muscle-specific promoter and is followed by the *HBB2* (Hemoglobin subunit β2) polyadenylation signal.

Adenovirus free rAAV2/9 viral preparations were generated by packaging AAV2-ITR recombinant genomes in AAV9 capsids, using a three plasmids transfection protocol as previously described (46). Briefly, HEK293 cells were cotransfected with pAAV-Des-m*Fkrp*, a RepCap plasmid (pAAV2.9, Dr J. Wilson, UPenn) and an adenoviral helper plasmid [(pXX6, (47)] at a ratio of 1:1:2. Crude viral lysate was harvested at 60 h post-transfection and lysed by freeze-and-thaw cycles. The viral lysate was purified through two rounds of CsCl ultracentrifugation followed by dialysis. Viral genomes were quantified by a TaqMan real-time PCR assay using primers and probes corresponding to the inverted terminal repeat region (ITR) of the AAV vector genome (48). The primer pairs and TaqMan probes used for ITR amplification were: 1AAV65/Fwd: 5′-CTCCATCACTA GGGGTTCCTTGTA-3′; 64AAV65/rev: 5′-TGGCTACGTAGATAAGT AGCATGGC-3′; and AAV65MGB/taq: 5′-GTTAATGATTAACCC-3′.

Cell culture and transfection

The human embryonic retinoblast HER911 cell line was cultured in DMEM (Thermo Fisher Scientific, Waltham, MA, USA) supplemented with 10% foetal bovine serum (FBS; Sigma, St. Louis, MO, USA), 10 μg/ml of gentamicin (Thermo Fisher Scientific, Waltham, MA, USA) plus 0.1% MEM non-essential amino acid solution (Sigma-Aldrich, St. Louis, MO, USA) for HER911 cells.

HER911 cells at a confluence of 70–80% were transfected using CaPO4-DNA complex, formed with the mixture of 2 μg of plasmid, 5 μl of CaCl2 2.5M, in HBS buffer (NaCl 140 mM, HEPES 50 mM, Na2HPO4 0.75 mM, NaOH 13.5 mM) per well. Cells were scrapped 48 h after transfection in the culture medium and centrifuged at 500 g, at 4 °C for 5 min. Cell pellets were stored at –80 °C until use.

RT-PCR and PCR analysis

RNA was extracted by the Trizol method (Thermo Fisher Scientific, Waltham, MA, USA) from muscles previously sampled and frozen in liquid nitrogen. Residual DNA was removed from the samples using the Free DNA kit according to the manufacturer's protocol (Thermo Fisher Scientific, Waltham, MA, USA). Quality of the purification was assessed by adding a control without reverse transcriptase in all experiments. One μg of RNA was reverse-transcribed using the RevertAid H Minus First Strand cDNA Synthesis Kit (Thermo Fisher Scientific, Waltham, MA, USA) and a mixture of random oligonucleotides and oligo-dT. Real-time PCR was performed using 7900HT Fast Real-Time PCR System (Thermo Fisher Scientific, Waltham, MA, USA) with 0.2 μM of each primer and 0.1 μM of the probe according to the protocol Absolute QPCR Rox Mix (Thermo Fisher Scientific, Waltham, MA, USA). The primers and Taqman probe (Eurogentec, Liège, Belgium) used for *Fkrp* gene expression assays were: 1303mFKRP.F (5′-CACCGGCAGGATGTTGAG TT-3′), 1376mFKRP.R (5′-GCCATGAAACCCGCAAAG-3′) and 1336 mFKRP.P (5′-CTGCAGCCACTTGTCCCCCTGC-3′). Data from the ubiquitous acidic ribosomal phosphoprotein (P0) was used to normalize the data across samples. The primer pairs and Taqman probe used for *P0* amplification were: m181PO.F (5′-CTCCAAGCAGATGCAGCAGA-3′), m267PO.R (5′-ACCATGATGCG CAAGGCCAT-3′) and m225PO.P (5′-CCGTGGTGCTGATGGGCAAGA A-3′). Each experiment was performed in duplicate.

For quantification of viral genomes on muscles, DNA was extracted from muscles previously sampled and frozen, using DNeasy Blood & Tissue Kit (Qiagen, Venlo, Nederlands). Real-time PCR was performed on 100 ng of DNA, using the same protocol as described above. Viral genome number of copies was determined by amplification of the ITR2 region of AAV genome (48). Primers and Taqman probe used were: forward 5′-CTCCATCACTAG GGGTTCCTTGTA-3′; reverse 5′-TGGCTACGTAGATAAGTAGCA TGGC-3′; and Taqman probe 5′-GTTAATGATTAACCC-3′. The values obtained for non-injected mouse muscles were subtracted to the ones obtained for the injected mouse muscles.

Western-blotting

Cell pellets and muscle tissues were mechanically homogenized in RIPA lysis buffer (Thermo Fisher Scientific, Waltham, MA, USA), complemented with Complete protease inhibitor cocktail EDTA-free (Roche, Bâle, Switzerland) or in 150 mM NaCl, 50 mM Tris, pH 7.4 (with a homemade cocktail of protease inhibitors), then solubilized with 1% Triton-X 100 as previously described (32). For αDG protein detection in FKRP mice, muscle homogenates were first boiled at 100 °C for 5 min, then centrifuged at 13 000 rpm for 15 min. Proteins were separated using precast polyacrylamide gel (anykD for αDG protein detection or 4–15% otherwise, BioRad, Hercules, CA, USA) and then transferred to nitrocellulose membrane. For the Ftkn experiments, large format 3–15% PAGE and transfer to PVDF-FL (Hoefer, Merck Millipore, Billerica, MA, USA) were used.

Rabbit polyclonal antibody against FKRP was generated through successive rounds of immunization with a peptide (KFGPGVIENPQYPNPALLSLTG) from the C-terminus of the human FKRP protein (Eurogentec, Liège, Belgium). Nitrocellulose membranes were probed with antibodies against FKRP (1:100), GAPDH (Santa Cruz Biotechnologies, Dallas, TX, USA, 1:200), αDG-IIH6 (Developmental Studies Hybridoma Bank (DSHB), Iowa City, IA, USA, 1:50, added with Merck Millipore, Billerica, MA, USA, 1:1000), βDG MANDAG2 (Developmental Studies Hybridoma Bank, Iowa City, IA, USA, 1:200), α-actinin (Santa Cruz Biotechnologies, Dallas, TX, USA, 1:300) or GRP78 (Abcam, Cambridge, UK, 1:1000) for 2 h at room temperature. Finally, membranes were incubated with IRDye® for detection by the Odyssey infrared-scanner (LI-COR Biosciences, Lincoln, NE, USA). For the Ftkn experiments, PVDF-FL membranes were probed with antibodies against FKRP (polyclonal Rbt 341) (1/100) (49), αDG-IIH6 (DSHB, 1/40); αDG core protein (1/100 concentrated supernatant (50), β-dystroglycan (βDG) MANDAG2 (DSHB, 1/100) and GAPDH (Cell Signaling Technologies, Danvers, MA, USA, 1/2000) overnight at 4 °C in 1% milk or casein TBS-T. After washing, blots were incubated for 1 h at room temperature with HRP-coupled secondary antibodies (Merck Millipore, Billerica, MA, USA, 1:4000) in 1% milk or casein TBS-T, washed, and imaged with SuperSignal West Pico or Dura (Thermo Fisher Scientific, Waltham, MA, USA) on the Fluorchem HD2 (Protein Simple, San Jose, CA, USA).

Methionine digestion of proteins

Protein homogenates were prepared as described above (Western blotting section). Proteins were concentrated 2-fold on an Amicon column (Amicon Ultra 2mL 3K, Merck Millipore,

Billerica, MA, USA) and separated using a NuPage pre-cast gel (4–12% Bis-Tris; Thermo Fisher Scientific, Waltham, MA, USA). After migration, pieces of gel containing either the 58 kDa or 42 kDa bands were sampled. Gel fragments were rinsed in water, washed once in formic acid, treated 45 min in cyanogen bromide (CNBr) at a concentration of 16 μg/μl, and finally neutralized in one bath of water followed by 4 baths of MOPS SDS running buffer (Thermo Fisher Scientific, Waltham, MA, USA) and a last bath of water. Proteins were then extracted from the gel slices by mechanical crushing in 0.1M sodium hydroxide. After incubation at 25 °C for 10 min, proteins were denatured and submitted to Western-blot.

Laminin overlay

Muscle proteins were prepared as described above for αDG protein detection, then separated and blotted on nitrocellulose membranes. The membranes were then blocked for 1 h at room temperature in laminin binding buffer (LBB: 10 mM triethanolamine, 140 mM NaCl, 1 mM $MgCl_2$, 1 mM $CaCl_2$, pH 7.6) complemented with 5% milk, and next incubated with 7.5 nM laminin 1 (Sigma, St. Louis, MO, USA, L2020) in LBB complemented with 3% BSA, at 4 °C for 16 h. After washes with TTBS buffer, the membranes were processed for a 2 h incubation with anti-laminin antibody (Agilent technologies, Glostrup, Denmark, 1:500) followed by 1 h incubation with HRP anti-rabbit antibody (GE Healthcare, Little Chalfont, UK, 1:5000). Blots were revealed by chemiluminescence (SuperSignal West Pico, Thermo Fisher Scientific, Waltham, MA, USA). A false color scheme (ImageJ:Red Hot) was applied to the images using ImageJ software.

Histology and immunohistochemistry

Skeletal and cardiac muscles were dissected out and frozen in isopentane cooled in liquid nitrogen. Transverse cryosections (7 or 10 μm thickness) were prepared from frozen muscles and were processed for Hematoxylin-Phloxine-Saffron (HPS) or Sirius Red histological stainings. For detection of Evans Blue-positive fibers, sections were fixed by cooled acetone and revealed by fluorescence excitation at 594 nm under a Leica microscope. Cartograph software (Microvision, Evry, France) was used to obtain mosaics of images. Centro-nucleated fibers and Evans Blue positive-areas were quantified using the Histolab software (Microvision, Evry, France) or ImagePro Insight (Media Cybernetics, Rockville, MD, USA).

The antibodies used for immuno-staining were CD3 (Abcam, Cambridge, UK, 1/400), CD11b (BD Biosciences, Franklin Lakes, NJ, USA, 1:40), βDG (DSHB, 1/40) and collagen VI (ColVI, Fitzgerald, Acton, MA, USA 1/1000) according to protocols previously described (49,50). For fluorescent intensity measurements, a region of interest was drawn around the entire psoas section and green intensity (ColVI or CD11b) was measured by the ImagePro Premier (MediaCybernetics).

In vivo injections

For intramuscular injections, male mice were injected into the TA muscle with a volume of 25 μl, or into the gastrocnemius or gluteus muscles with a volume of 50 μl divided between 2 sites of injection. For intravenous injections into $FKRP^{L276I}$ mice, a volume of 200 μl containing the AAV vector was injected into the tail vein. A volume of ∼70–90 μl (low dose) or ∼110–140 μl (high dose) of rAAV9-*mFkrp* or 140 μl of 0.9% sterile saline control were injected into the tail vein of 4 week old Myf5/Fktn knock-out or littermate controls mice based on body weight.

Functional tests

Ex vivo measure of specific force of the EDL and soleus was performed as previously described (51). A protocol of large strength injury (LSI) (28,29) was used. First, mice were intraperitoneally injected with Evans blue dye (EBD, 0.1 mg/10g of body weight). Eight hours after injection, the mice were placed on a rig and were submitted to a 300 ms stimulation of the sciatic nerve, inducing tetanus of the ankle dorsiflexor group of muscles; 150 ms after onset of stimulation, the ankle was plantarflexed from 90 to 175° at an angular velocity of 1200°/s. This exercise was repeated 15 times, with a 2-min rest between successive lengthening contractions. The following day, the mice were sacrificed and the TA muscles were removed and quickly frozen in liquid nitrogen-cooled isopentane.

Statistical analysis

Bar graphs, dot plots and fiber area plots show mean +/- standard error of the mean (SEM). Comparisons of quantitative data between groups were performed using the Wilcoxon-Mann-Whitney test (R software) or two-way ANOVA for Myf5/Fktn genotype vs. dose with Bonferonni's post-test (Prism 5, GraphPad). Statistical significance is represented by stars on the graphs respecting these rules: (*) for P-value < 0.05, (**) for P-value < 0.01 and (***) for P-value < 0.001. Outlier analysis was performed using the ROUT and Grubbs tests using GraphPad Prism 5.

Supplementary Material

Supplementary Material is available at *HMG* online.

Acknowledgements

This work was supported by the AFM (Association Française contre les Myopathies; 1 rue de l'Internationale, 91002 Evry, France), the LGMD2I fund (LGMD2i Research Fund; PO Box 245, Bellevue, WA 98009, USA) and the University of Georgia College of Pharmacy (University of Georgia College of Pharmacy; 250 W. Green Street, Athens, Georgia 30602, USA). We would like to thank Dr. Claudia Mitchell for helpful discussion, Dr. Susan Brown (Royal Veterinarian College, London UK) for the αDG WB technology, Dr Nathalie Daniele for help during the generation of the mouse model, Dr Pasqualina Colella for providing samples, Gautier Sobczak, Giorgio Gargari, Marine Faivre and Junna Luan for technical assistance and Sian Cronin for critical reading of the manuscript. We acknowledge the help of the Genethon support teams for AAV production, *in vivo* experimentation and histology and the 'Mouse Clinic Institute' (MCI/ICS; Illkirch) for the generation of the FKRP model.

Conflict of Interest statement. None declared.

Funding

This work was supported by the Association Française contre les Myopathies (AFM) and the University of Georgia College of Pharmacy. We benefited from funding by the LGMD2i Research Fund.

References

1. Barresi, R. and Campbell, K.P. (2006) Dystroglycan: from biosynthesis to pathogenesis of human disease. *J. Cell Sci.*, **119**, 199–207.
2. Talts, J.F., Andac, Z., Gohring, W., Brancaccio, A. and Timpl, R. (1999) Binding of the G domains of laminin alpha1 and alpha2 chains and perlecan to heparin, sulfatides, alpha-dystroglycan and several extracellular matrix proteins. *EMBO J.*, **18**, 863–870.
3. Hohenester, E., Tisi, D., Talts, J.F. and Timpl, R. (1999) The crystal structure of a laminin G-like module reveals the molecular basis of alpha-dystroglycan binding to laminins, perlecan, and agrin. *Mol. Cell*, **4**, 783–792.
4. Tisi, D., Talts, J.F., Timpl, R. and Hohenester, E. (2000) Structure of the C-terminal laminin G-like domain pair of the laminin alpha2 chain harbouring binding sites for alpha-dystroglycan and heparin. *EMBO J.*, **19**, 1432–1440.
5. Ervasti, J.M. and Campbell, K.P. (1993) A role for the dystrophin-glycoprotein complex as a transmembrane linker between laminin and actin. *J. Cell. Biol*, **122**, 809–823.
6. Gee, S.H., Montanaro, F., Lindenbaum, M.H. and Carbonetto, S. (1994) Dystroglycan-alpha, a dystrophin-associated glycoprotein, is a functional agrin receptor. *Cell*, **77**, 675–686.
7. Peng, H.B., Ali, A.A., Daggett, D.F., Rauvala, H., Hassell, J.R. and Smalheiser, N.R. (1998) The relationship between perlecan and dystroglycan and its implication in the formation of the neuromuscular junction. *Cell Adhes. Commun.*, **5**, 475–489.
8. Sugita, S., Saito, F., Tang, J., Satz, J., Campbell, K. and Sudhof, T.C. (2001) A stoichiometric complex of neurexins and dystroglycan in brain. *J. Cell. Biol*, **154**, 435–445.
9. Sato, S., Omori, Y., Katoh, K., Kondo, M., Kanagawa, M., Miyata, K., Funabiki, K., Koyasu, T., Kajimura, N., Miyoshi, T. *et al.* (2008) Pikachurin, a dystroglycan ligand, is essential for photoreceptor ribbon synapse formation. *Nat. Neurosci.*, **11**, 923–931.
10. Endo, T. (2015) Glycobiology of alpha-dystroglycan and muscular dystrophy. *J. Biochem.*, **157**, 1–12.
11. Breton, C. and Imberty, A. (1999) Structure/function studies of glycosyltransferases. *Curr. Opin. Struct. Biol*, **9**, 563–571.
12. Brockington, M., Blake, D.J., Prandini, P., Brown, S.C., Torelli, S., Benson, M.A., Ponting, C.P., Estournet, B., Romero, N.B., Mercuri, E. *et al.* (2001) Mutations in the fukutin-related protein gene (FKRP) cause a form of congenital muscular dystrophy with secondary laminin alpha2 deficiency and abnormal glycosylation of alpha-dystroglycan. *Am. J. Hum. Genet*, **69**, 1198–1209.
13. Kanagawa, M., Kobayashi, K., Tajiri, M., Manya, H., Kuga, A., Yamaguchi, Y., Akasaka-Manya, K., Furukawa, J., Mizuno, M., Kawakami, H. *et al.* (2016) Identification of a Post-translational Modification with Ribitol-Phosphate and Its Defect in Muscular Dystrophy. *Cell Rep.*, **14**(9), 2209–2223.
14. Brockington, M., Yuva, Y., Prandini, P., Brown, S.C., Torelli, S., Benson, M.A., Herrmann, R., Anderson, L.V., Bashir, R., Burgunder, J.M. *et al.* (2001) Mutations in the fukutin-related protein gene (FKRP) identify limb girdle muscular dystrophy 2I as a milder allelic variant of congenital muscular dystrophy MDC1C. *Hum. Mol. Genet.*, **10**, 2851–2859.
15. Beltran-Valero de Bernabe, D., Voit, T., Longman, C., Steinbrecher, A., Straub, V., Yuva, Y., Herrmann, R., Sperner, J., Korenke, C., Diesen, C. *et al.* (2004) Mutations in the FKRP gene can cause muscle-eye-brain disease and Walker-Warburg syndrome. *J. Med. Genet.*, **41**, e61.
16. Mercuri, E., Brockington, M., Straub, V., Quijano-Roy, S., Yuva, Y., Herrmann, R., Brown, S.C., Torelli, S., Dubowitz, V., Blake, D.J. *et al.* (2003) Phenotypic spectrum associated with mutations in the fukutin-related protein gene. *Ann. Neurol.*, **53**, 537–542.
17. Walter, M.C., Petersen, J.A., Stucka, R., Fischer, D., Schroder, R., Vorgerd, M., Schroers, A., Schreiber, H., Hanemann, C.O., Knirsch, U. *et al.* (2004) FKRP (826C>A) frequently causes limb-girdle muscular dystrophy in German patients. *J. Med. Genet.*, **41**, e50.
18. Sveen, M.L., Schwartz, M. and Vissing, J. (2006) High prevalence and phenotype-genotype correlations of limb girdle muscular dystrophy type 2I in Denmark. *Ann. Neurol.*, **59**, 808–815.
19. Stensland, E., Lindal, S., Jonsrud, C., Torbergsen, T., Bindoff, L.A., Rasmussen, M., Dahl, A., Thyssen, F. and Nilssen, O. (2010) Prevalence, mutation spectrum and phenotypic variability in Norwegian patients with Limb Girdle Muscular Dystrophy 2I. *Neuromuscul. Disord.*, **21**, 41–46.
20. Margeta, M., Connolly, A.M., Winder, T.L., Pestronk, A. and Moore, S.A. (2009) Cardiac pathology exceeds skeletal muscle pathology in two cases of limb-girdle muscular dystrophy type 2I. *Muscle Nerve*, **40**, 883–889.
21. Muller, T., Krasnianski, M., Witthaut, R., Deschauer, M. and Zierz, S. (2005) Dilated cardiomyopathy may be an early sign of the C826A Fukutin-related protein mutation. *Neuromuscul. Disord.*, **15**, 372–376.
22. D'Amico, A., Petrini, S., Parisi, F., Tessa, A., Francalanci, P., Grutter, G., Santorelli, F.M. and Bertini, E. (2008) Heart transplantation in a child with LGMD2I presenting as isolated dilated cardiomyopathy. *Neuromuscul. Disord.*, **18**, 153–155.
23. Wahbi, K., Meune, C., Hamouda el, H., Stojkovic, T., Laforet, P., Becane, H.M., Eymard, B. and Duboc, D. (2008) Cardiac assessment of limb-girdle muscular dystrophy 2I patients: an echography, Holter ECG and magnetic resonance imaging study. *Neuromuscul. Disord.*, **18**, 650–655.
24. Gaul, C., Deschauer, M., Tempelmann, C., Vielhaber, S., Klein, H.U., Heinze, H.J., Zierz, S. and Grothues, F. (2006) Cardiac involvement in limb-girdle muscular dystrophy 2I: conventional cardiac diagnostic and cardiovascular magnetic resonance. *J. Neurol.*, **253**, 1317–1322.
25. Xu, L., Lu, P.J., Wang, C.H., Keramaris, E., Qiao, C., Xiao, B., Blake, D.J., Xiao, X. and Lu, Q.L. (2013) Adeno-associated virus 9 mediated FKRP gene therapy restores functional glycosylation of alpha-dystroglycan and improves muscle functions. *Mol. Ther.: J. Am. Soc. Gene Ther.*, **21**, 1832–1840.
26. Qiao, C., Wang, C.H., Zhao, C., Lu, P., Awano, H., Xiao, B., Li, J., Yuan, Z., Dai, Y., Martin, C.B. *et al.* (2014) Muscle and heart function restoration in a limb girdle muscular dystrophy 2I (LGMD2I) mouse model by systemic FKRP gene delivery. *Mol. Ther.: J. Am. Soc. Gene Ther.*, **22**, 1890–1899.
27. Alhamidi, M., Kjeldsen Buvang, E., Fagerheim, T., Brox, V., Lindal, S., Van Ghelue, M. and Nilssen, O. (2011) Fukutin-related protein resides in the Golgi cisternae of skeletal muscle fibres and forms disulfide-linked homodimers via an N-terminal interaction. *PloS One*, **6**, e22968.
28. Roche, J.A., Lovering, R.M. and Bloch, R.J. (2008) Impaired recovery of dysferlin-null skeletal muscle after contraction-induced injury in vivo. *Neuroreport*, **19**, 1579–1584.
29. Roche, J.A., Lovering, R.M., Roche, R., Ru, L.W., Reed, P.W. and Bloch, R.J. (2010) Extensive mononuclear infiltration and myogenesis characterize recovery of dysferlin-null skeletal muscle from contraction-induced injuries. *Am. J. Physiol. Cell. Physiol*, **298**, C298–C312.

30. Boito, C.A., Fanin, M., Gavassini, B.F., Cenacchi, G., Angelini, C. and Pegoraro, E. (2007) Biochemical and ultrastructural evidence of endoplasmic reticulum stress in LGMD2I. *Virchows Arch.*, **451**, 1047–1055.
31. Lin, Y.Y., White, R.J., Torelli, S., Cirak, S., Muntoni, F. and Stemple, D.L. (2011) Zebrafish Fukutin family proteins link the unfolded protein response with dystroglycanopathies. *Hum. Mol. Genet.*, **20**, 1763–1775.
32. Beedle, A.M., Turner, A.J., Saito, Y., Lueck, J.D., Foltz, S.J., Fortunato, M.J., Nienaber, P.M. and Campbell, K.P. (2012) Mouse fukutin deletion impairs dystroglycan processing and recapitulates muscular dystrophy. *J. Clin. Invest.*, **122**, 3330–3342.
33. Esapa, C.T., McIlhinney, R.A. and Blake, D.J. (2005) Fukutin-related protein mutations that cause congenital muscular dystrophy result in ER-retention of the mutant protein in cultured cells. *Hum. Mol. Genet.*, **14**, 295–305.
34. Keramaris-Vrantsis, E., Lu, P.J., Doran, T., Zillmer, A., Ashar, J., Esapa, C.T., Benson, M.A., Blake, D.J., Rosenfeld, J. and Lu, Q.L. (2007) Fukutin-related protein localizes to the Golgi apparatus and mutations lead to mislocalization in muscle in vivo. *Muscle Nerve*, **36**, 455–465.
35. Dolatshad, N.F., Brockington, M., Torelli, S., Skordis, L., Wever, U., Wells, D.J., Muntoni, F. and Brown, S.C. (2005) Mutated fukutin-related protein (FKRP) localises as wild type in differentiated muscle cells. *Exp. Cell Res.*, **309**, 370–378.
36. Krag, T.O. and Vissing, J. (2015) A new mouse model of limb-girdle muscular dystrophy type 2I homozygous for the common L276I mutation mimicking the mild phenotype in humans. *J. Neuropathol. Exp. Neurol.*, **74**, 1137–1146.
37. Barresi, R., Michele, D.E., Kanagawa, M., Harper, H.A., Dovico, S.A., Satz, J.S., Moore, S.A., Zhang, W., Schachter, H., Dumanski, J.P. *et al.* (2004) LARGE can functionally bypass alpha-dystroglycan glycosylation defects in distinct congenital muscular dystrophies. *Nat. Med.*, **10**, 696–703.
38. Brockington, M., Torelli, S., Sharp, P.S., Liu, K., Cirak, S., Brown, S.C., Wells, D.J. and Muntoni, F. (2010) Transgenic overexpression of LARGE induces alpha-dystroglycan hyperglycosylation in skeletal and cardiac muscle. *PloS One*, **5**, e14434.
39. Vannoy, C.H., Xu, L., Keramaris, E., Lu, P., Xiao, X. and Lu, Q.L. (2014) Adeno-associated virus-mediated overexpression of LARGE rescues alpha-dystroglycan function in dystrophic mice with mutations in the fukutin-related protein. *Hum. Gene Ther. Methods*, **25**, 187–196.
40. Goddeeris, M.M., Wu, B., Venzke, D., Yoshida-Moriguchi, T., Saito, F., Matsumura, K., Moore, S.A. and Campbell, K.P. (2013) LARGE glycans on dystroglycan function as a tunable matrix scaffold to prevent dystrophy. *Nature*, **503**, 136–140.
41. Whitmore, C., Fernandez-Fuente, M., Booler, H., Parr, C., Kavishwar, M., Ashraf, A., Lacey, E., Kim, J., Terry, R., Ackroyd, M.R. *et al.* (2014) The transgenic expression of LARGE exacerbates the muscle phenotype of dystroglycanopathy mice. *Hum. Mol. Genet.*, **23**, 1842–1855.
42. Jimenez-Mallebrera, C., Torelli, S., Feng, L., Kim, J., Godfrey, C., Clement, E., Mein, R., Abbs, S., Brown, S.C., Campbell, K.P. *et al.* (2009) A comparative study of alpha-dystroglycan glycosylation in dystroglycanopathies suggests that the hypoglycosylation of alpha-dystroglycan does not consistently correlate with clinical severity. *Brain Pathol.*, **19**, 596–611.
43. Saito, F., Kanagawa, M., Ikeda, M., Hagiwara, H., Masaki, T., Ohkuma, H., Katanosaka, Y., Shimizu, T., Sonoo, M., Toda, T. *et al.* (2014) Overexpression of LARGE suppresses muscle regeneration via down-regulation of insulin-like growth factor 1 and aggravates muscular dystrophy in mice. *Hum. Mol. Genet.*, **23**, 4543–4558.
44. Chan, Y.M., Keramaris-Vrantsis, E., Lidov, H.G., Norton, J.H., Zinchenko, N., Gruber, H.E., Thresher, R., Blake, D.J., Ashar, J., Rosenfeld, J. *et al.* (2010) Fukutin-related protein is essential for mouse muscle, brain and eye development and mutation recapitulates the wide clinical spectrums of dystroglycanopathies. *Hum. Mol. Genet.*, **19**, 3995–4006.
45. Foltz, S.J., Melick, G.A., Abousaud, M.I., Luan, J., Fortunato, M.J. and Beedle, A.M. (2016) Abnormal skeletal muscle regeneration plus mild alterations in mature fiber type specification in fktn-deficient dystroglycanopathy muscular dystrophy mice. *PloS One*, **11**, e0147049.
46. Bartoli, M., Poupiot, J., Goyenvalle, A., Perez, N., Garcia, L., Danos, O. and Richard, I. (2006) Noninvasive monitoring of therapeutic gene transfer in animal models of muscular dystrophies. *Gene Ther.*, **13**, 20–28.
47. Apparailly, F., Khoury, M., Vervoordeldonk, M.J., Adriaansen, J., Gicquel, E., Perez, N., Riviere, C., Louis-Plence, P., Noel, D., Danos, O. *et al.* (2005) Adeno-associated virus pseudotype 5 vector improves gene transfer in arthritic joints. *Hum. Gene Ther.*, **16**, 426–434.
48. Rohr, U.P., Wulf, M.A., Stahn, S., Steidl, U., Haas, R. and Kronenwett, R. (2002) Fast and reliable titration of recombinant adeno-associated virus type-2 using quantitative real-time PCR. *J. Virol. Methods*, **106**, 81–88.
49. Beedle, A.M., Nienaber, P.M. and Campbell, K.P. (2007) Fukutin-related protein associates with the sarcolemmal dystrophin-glycoprotein complex. *J. Biol. Chem.*, **282**, 16713–16717.
50. Fortunato, M.J., Ball, C.E., Hollinger, K., Patel, N.B., Modi, J.N., Rajasekaran, V., Nonneman, D.J., Ross, J.W., Kennedy, E.J., Selsby, J.T. *et al.* (2014) Development of rabbit monoclonal antibodies for detection of alpha-dystroglycan in normal and dystrophic tissue. *PloS One*, **9**, e97567.
51. Fougerousse, F., Gonin, P., Durand, M., Richard, I. and Raymackers, J.M. (2003) Force impairment in calpain 3-deficient mice is not correlated with mechanical disruption. *Muscle Nerve*, **27**, 616–623.